Crystal Growth of Quaternary Rare Earth Selenosilicates by Using the Flux-Assisted Boron Chalcogen Mixture Method: Investigation of their Magnetic and Optical Properties

Habiba Binte Kashem[1], Gopabandhu Panigrahi[1], Gregory Morrison[1], Eric A. Gabilondo[2], P. Shiv Halasyamani[2], Pandu Wisesa[3], Theodore M. Besmann[3], and Hans-Conrad zur Loye[1*]

[1]Department of Chemistry and Biochemistry, University of South Carolina, Columbia, SC, 29208, United States

[2]Department of Chemistry, University of Houston, Houston, TX, 77204, United States

[3]Department of Mechanical Engineering, University of South Carolina, Columbia, SC, 29208, United States

*E-mail: zurloye@mailbox.sc.edu

Abstract:

A series of rare earth magnesium selenosilicates, $RE_3Mg_{0.5}SiSe_7$ (*RE* = Ce, Pr, Nd, Sm, Gd, Tb, Dy) were obtained as single crystal using the flux assisted boron chalcogen mixture (BCM) method. The structures of the crystals were determined by single-crystal X-ray diffraction. The $RE_3Mg_{0.5}SiSe_7$ series crystallizes in the hexagonal crystal system in the space group $P6_3$. Polycrystalline powders were synthesized to perform physical property measurements. Magnetic measurements over the 2-300 K temperature range reveal that $Ce_3Mg_{0.5}SiSe_7$ and $Gd_3Mg_{0.5}SiSe_7$ exhibit paramagnetic behavior with negative Weiss constants (θ_W = -14.50, θ_W = -6.13 K, respectively). The optical properties of $RE_3Mg_{0.5}SiSe_7$ (*RE* = Ce, Pr, Nd, Sm, Gd) were measured by UV-visible diffuse reflectance. DFT electronic structure calculations were performed. A second harmonic generation measurement was performed on a polycrystalline powder of $Ce_3Mg_{0.5}SiSe_7$ and was found to be SHG active with an efficiency of 0.11 times the standard potassium dihydrogen phosphate (KDP).

Introduction

Chalcogenides exhibit extremely high structural and compositional diversity, only surpassed by organic compounds and metal oxides and, consequently, the synthesis of complex metal chalcogenides has been widely explored to take advantage of the extensive physical properties resulting from their structural diversity.[1-3] Among multicomponent systems, complex rare-earth chalcogenides have occupied an important place due to the ability of lanthanide-containing chalcogenides to form intricate ternary and quaternary compounds with a broad range of crystal structures and chemical compositions. These novel structures of metal chalcogenides can exhibit properties that enable their use in various applications, including nonlinear optical materials (NLO),[4, 5] photoluminescence,[6] magnetism,[7, 8] scintillation,[9] fast ion conductor,[10, 11] thermoelectric,[12] and radiation detectors.[13, 14] Although these materials have great potential for use in applications, there exist numerous synthetic challenges due to the high reactivity of rare earth metal reagents toward oxygen and moisture, as well as the limited availability of rare earth chalcogenide reagents. The zur Loye group has been addressing these challenges by using the boron chalcogen mixture (BCM) method, which allows for the in-situ conversion of metal oxide precursors to metal chalcogenides, thereby avoiding the need for metal chalcogenide starting reagents.[15-17] Many actinide and lanthanide containing chalcogenides have already been reported using the BCM method as the synthetic route. [6, 18-21]

Among the well-known rare-earth chalcogenides, the quaternary novel rare earth chalcogenides family, $RE_3M_{0.5}TQ_7$ (M = Metal, T = Si, Ge, Q = S, Se) has received increasing attention due to the ability to accommodate elemental substitutions that are facilitated by the structural flexibility that can impart specific optical, magnetic, and ionic conducting behavior.[8, 22-33] In this chalcogenide family, the metal atom can have full occupancy by taking on a trigonal planar coordination environment,[34, 35] or can have half occupancy in an octahedral coordination environment,[36] making this family structurally and compositionally quite flexible. Among the $RE_3M_{0.5}TQ_7$ family, the magnesium series, $RE_3Mg_{0.5}TQ_7$, has not been intensively studied. Recently the zur Loye group published on a series of rare earth magnesium thiosilicates prepared by applying the flux-assisted BCM technique.[33] For the selenium analogs, $Ce_3Mg_{0.5}SiSe_7$ and $Pr_3Mg_{0.5}SiSe_7$ are the only compositions reported so far.[31]

We, therefore, decided to investigate the selenium analogs of this series to explore their optical and magnetic properties. Changing from S to Se, is accompanied by an increase in the size, a decrease in the electronegativity, and an increase in the metallic nature of these elements, potentially resulting in changes to their physical properties. Furthermore, Mg^{2+} being diamagnetic and optically inactive will enable us to investigate the behavior of only the rare earth elements in this structure. Many compounds from this family, including the title compounds, crystallize in the noncentrosymmetric space group $P6_3$, making these structures potentially SHG active and, thus, of interest for nonlinear optical properties (NLO).

To date, the preparation of most $RE_3M_{0.5}TQ_7$ (M = Metal, T = Si, Ge, Q = S, Se) compounds was accomplished via a solid state synthesis route by heating the reactants in an evacuated fused-silica tube, although others were prepared via molten flux synthesis and the boron chalcogen mixture (BCM) method.[8, 19, 37] In our exploration, we decided to take advantage of the combined BCM and molten flux methods to target single crystals of the $RE_3Mg_{0.5}SiSe_7$ (*RE* = Ce, Pr, Nd, Sm, Gd, Tb, Dy) series to enable structure determination, while the combined BCM method and solid state synthesis route was used to obtain polycrystalline samples for property measurements. Herein, we discuss the synthetic approach for obtaining high-quality single crystals of $RE_3Mg_{0.5}SiSe_7$ (*RE* = Ce, Pr, Nd, Sm, Gd, Tb, Dy) along with their crystal structure determinations, and furthermore, we report on our investigation of the magnetic properties of $RE_3Mg_{0.5}SiSe_7$ (*RE* = Ce, Gd), and the SHG properties of $Ce_3Mg_{0.5}SiSe_7$ compounds within this series.

Experimental Section

RE_2O_3 (RE = Nd, Sm, Gd, Dy) (99.9%, Alfa Aesar), CeO_2 (99.9%, Alfa Aesar), Pr_6O_{11} (99.9% Alfa Aesar), Tb_4O_7 (99.9% Alfa Aesar), selenium (99.9% Fisher Scientific), boron (crystalline 100 mesh, 99.9%, Beantown Chemical), SiO_2 (amorphous powder, 99.9%, Alfa Aesar), MgO (99.9% Alfa Aesar), NaI (99.9%, Beantown Chemical) reagents were used as received for the synthesis of the targeted compounds. NaI was stored in a drying oven overnight set to 260 °C to ensure that NaI was anhydrous.

Single crystals of $RE_3Mg_{0.5}SiSe_7$ (*RE* = Ce, Pr, Nd, Sm, Gd, Tb, Dy) compounds were synthesized by the addition of 50 mg of RE_2O_3 (*RE* = Nd, Sm, Gd, Dy), CeO_2, Pr_6O_{11}, or Tb_4O_7, 45 mg of selenium, 10 mg of boron, 5 mg of SiO_2, and 2 mg of MgO powders into a heavily

carbon coated fused silica tube (10 mm × 12 mm inner and outer diameters) along with 250 mg of NaI flux. The fused silica tube was evacuated to 10^{-4} torr and flame-sealed using a methane/oxygen torch. The sealed fused silica tube was placed into a programmable furnace, heated to 760 °C in 20 h, kept at this temperature for 20 h and cooled to 560 °C in 20 h, at which point the furnace was shut off and allowed to cool down to room temperature.

To prepare samples for property measurements, solid-state syntheses of $RE_3Mg_{0.5}SiSe_7$ (*RE* = Ce, Pr, Nd, Sm, Gd), were performed using the BCM method. The same materials were used as for the flux reactions, however, in the absence of the flux. For these reactions, RE_2O_3 (*RE* = Nd, Sm, Gd), CeO_2, or Pr_6O_{11}, boron, selenium, SiO_2, and MgO powders were used in a 1.5 (3 for CeO_2, and 0.5 for Pr_6O_{11}):10:7:1:0.5 molar ratio. The reactants were intimately ground using a mortar and pestle, and the ground mixture was added to a carbon-coated fused silica tube. The evacuated and sealed fused silica tube was then placed into a programmable furnace set to ramp to 950 °C in 2 h and dwelled for 20 h, at which point the furnace was shut off and allowed to return to room temperature. The resulting products were washed three times with methanol and were sonicated to remove any remaining impurities. All the products exhibited air and moisture stability. The powder X-ray diffraction analyses Figures S1-S5 confirmed the phase purity of the samples that were used for physical property measurements.

Caution. *Boron selenides are moisture-sensitive which leads to the generation of H_2Se gas upon contact with moisture and water. Therefore, all reaction work needs to be conducted in fume hood with the proper safety protocols.*

Single-Crystal X-ray Diffraction (SXRD).

Single-crystal X-ray diffraction data of the $RE_3Mg_{0.5}SiSe_7$ (*RE* = Ce, Pr, Nd, Sm, Gd, Tb, Dy) series were collected on a Bruker D8 QUEST diffractometer equipped with a PHOTON-II area detector and an Incoatec microfocus radiation source (Mo Kα radiation, λ = 0.71073 Å). Suitable size single crystals were mounted on a microloop using immersion oil. For collecting the data, the detector to crystal distance was fixed to 40 mm and 10 s/frame exposure time was used. The raw area detector data frames were reduced and corrected for absorption effects using the SAINT and SADABS programs.[38]

Final unit cell parameters were determined by the least-squares refinement of large sets of reflections from each data set.[39] An initial structural model was obtained with SHELXT. Subsequent difference Fourier calculations and full-matrix least-squares refinement against F^2 were performed with SHELXL[40] using the Olex2 interface.[41] All compounds crystallize in the non-centrosymmetric, hexagonal space group $P6_3$. The asymmetric unit contains three selenium atoms, one magnesium atom, one lanthanide atom, and one silicon atom. All atoms were refined with anisotropic displacement parameters. The Mg occupancy refined in all cases to essentially 0.5 within standard deviation (0.496(5) for $Gd_3Mg_{0.5}SiSe_7$) and was therefore fixed at 0.5. The crystallographic data and diffraction results are provided in Table 1.

Powder X-ray Diffraction (PXRD).

Powder X-ray diffraction (PXRD) patterns were collected using finely ground polycrystalline samples of $RE_3Mg_{0.5}SiSe_7$ (*RE* = Ce, Pr, Nd, Sm, Gd) prepared by the solid-state synthesis (Figures S1-S5). PXRD data were collected on a Bruker D2 PHASER diffractometer using Cu−Kα radiation (λ = 1.5418 Å) over the 2θ range 5−65° with a step size of 0.02°. Some minor RE_3Se_4 (*RE* = Pr, Sm) peaks were observed in the diffraction patterns of $Pr_3Mg_{0.5}SiSe_7$ and $Sm_3Mg_{0.5}SiSe_7$, and several unmatched reflections were observed in the $Gd_3Mg_{0.5}SiSe_7$ diffraction pattern.

Table 1. Crystallographic Data and Diffraction Results for $RE_3Mg_{0.5}SiSe_7$ Compounds

Chemical formula	$Ce_3Mg_{0.5}SiSe_7$	$Pr_3Mg_{0.5}SiSe_7$	$Nd_3Mg_{0.5}SiSe_7$	$Sm_3Mg_{0.5}SiSe_7$	$Gd_3Mg_{0.5}SiSe_7$	$Tb_3Mg_{0.5}SiSe_7$	$Dy_3Mg_{0.5}SiSe_7$
Formula weight	1013.33	1015.70	1025.68	1044.02	1064.71	1069.73	1080.46
Crystal system	Hexagonal						
Space group	$P6_3$						
Temperature (K)	301	299	298	299	299	297	298
***a* (Å)**	10.6645(1)	10.5950(1)	10.5430(2)	10.4408(2)	10.3644(2)	10.3010(1)	10.2428(1)
c (Å)	5.9880(1)	5.9733(1)	5.9621(1)	5.9391(1)	5.9309(1)	5.9374(1)	5.9545(1)
***V* (Å^3)**	589.785(15)	580.693(15)	573.93(2)	560.69(2)	551.75(2)	545.614(14)	541.020(14)
Z	2						
μ (mm^{-1})	33.050	34.394	35.636	38.297	40.984	42.654	44.125
Crystal size (mm)	0.03 × 0.03× 0.03	0.05 × 0.02 × 0.01	0.01 × 0.01× 0.01	0.02 × 0.01 × 0.01	0.05 × 0.03 × 0.01	0.05 × 0.04 × 0.01	0.05 × 0.02 × 0.01
ρ_{calcd} (g/cm^3)	5.706	5.809	5.935	6.184	6.409	6.511	6.632
Radiation (λ, Å)	Mo Kα (λ = 0.71073)						
2θ range, deg	4.41 – 72.748	4.44 - 72.66	4.462 - 72.734	4.504 - 72.7	4.538 - 72.72	4.566 - 72.686	4.592 - 72.698
Reflections collected	33907	38250	35469	32030	31629	31318	30786
R_{int}	0.0334	0.0354	0.0411	0.0562	0.0322	0.0343	0.0297
GOF (F^2)	1.092	1.113	1.205	1.153	1.179	1.108	1.190
R_1 ($I > 2\sigma(I)$)	0.0080	0.0088	0.0126	0.0185	0.0075	0.0081	0.0085
wR_2 (all data)	0.0157	0.0184	0.0267	0.0315	0.0165	0.0184	0.0192
$\Delta\rho_{max}$, $\Delta\rho_{min}$ (e Å^{-3})	0.39/-0.40	0.50/-0.51	0.71/-0.65	1.61/-1.04	0.39/-0.48	0.45/-0.70	0.70/-0.60
Flack parameter	0.039(8)	0.037(10)	0.035(16)	0.040(3)	0.045(13)	0.037(15)	0.027(18)

Energy-Dispersive X-ray Spectroscopy (EDS).

To collect EDS data on a single crystal, the crystal was mounted directly onto a SEM stub with carbon tape. Quantitative elemental analysis was performed by using a TESCAN Vega-3 SBU scanning electron microscope (SEM) with a Thermo EDS attachment, which is operated in low vacuum mode. Crystals were analyzed using a 15-20 kV accelerating voltage and a 40 s accumulation time. The summarized EDS data are provided in the Table S1.

UV-vis Spectroscopy.

UV−vis diffuse reflectance spectra, for $RE_3Mg_{0.5}SiSe_7$ (*RE* = Ce, Pr, Nd, Sm, Gd) were obtained using a PerkinElmer Lambda 35 UV−vis spectrophotometer equipped with an integrating sphere. Spectra were recorded over the 300-900 nm range at room temperature. The Kubelka-Munk function was used to convert the reflectance data to absorbance.[42]

Magnetic Susceptibility.

Magnetic property measurements of $Ce_3Mg_{0.5}SiSe_7$ and $Gd_3Mg_{0.5}SiSe_7$ were performed using a Quantum Design magnetic property measurement system (QD MPMS 3 SQUID Magnetometer). The magnetic susceptibility was measured in an applied magnetic field of 0.1 T under zero-field-cooled (zfc) and field-cooled (fc) conditions from 2 to 300 K. Magnetization as a function of the applied field was measured from -5 to 5 T at 2 K. Data were corrected for the sample shape and radial offset effects as described previously.[43]

Second-Harmonic Generation (SHG).

Powder SHG response of $Ce_3Mg_{0.5}SiSe_7$ was measured with a modified Kurtz−Perry system[44, 45] using a Nd:YAG solid-state laser at 1064 nm with KH_2PO_4 (KDP) in the particle size range 90−125 μm serving as the reference.

Computational Details:

To further discern the electronic structures of these novel materials we performed density functional theory calculations on $RE_3Mg_{0.5}SiSe_7$ (*RE* = Pr, Nd, Sm, Gd). The DFT calculations were carried out using the Vienna *Ab initio* Simulation Package (VASP).[46-48] The Kohn-Sham equations were solved within periodic boundary conditions with the r^{2}SCAN[49] exchange correlation. r^{2}SCAN is chosen as metaGGA has been found to provide a more accurate material property values compared to the widely used GGA functionals,[50] such as Perdew-Burke-

Ernzerhof (PBE)[51] which has a tendency to underbind[52] for a wide array of materials.[53, 54] The Brillouin zone was sampled such that the smallest distance in the *k*-grid was set to be 0.12.[55, 56] The self-consistent electronic loop was set to terminate at a tolerance of at least 10^{-5} eV, the ionic relaxation was set to converge at 10^{-3} eVthe planewave cutoff was set to be 520 eV. These cutoff values are set to be sufficiently tight to ensure proper representation of the electronic properties of the materials.[57] The phonon modes were calculated using density functional perturbation theory (DFPT) and the results analyzed with phonopy.[58, 59]

Results and Discussion:

Synthesis:

The family of $RE_3M_{0.5}TQ_7$ phases has been extensively explored since the early 2000s, due to interest in its structural and compositional diversity. A review of $RE_3M_{0.5}TQ_7$ compounds reveals that while many phases belonging to this family have already been explored, most of the reported phases are sulfides with only very little exploration of selenides. We targeted the synthesis of selenides, $RE_3Mg_{0.5}SiSe_7$, to further test the limits of the BCM method and to increase our understanding of the crystal chemistry of the $RE_3M_{0.5}TQ_7$ family. The known compositions of the $RE_3M_{0.5}TSe_7$ (M = Metal, T = Si, Ge) structure type are compiled in Table 2.

Table 2. Known selenosilicate and selenogermanate compounds of the $RE_3M_{0.5}TSe_7$ series

	RE^{3+}										
M^{2+}	La	Ce	Pr	Nd	Sm	Gd	Tb	Dy	Ho	Er	ref
Mg^{2+}		■ ●	■ ●								31
Mn^{2+}	■	●			■						37
Fe^{2+}	■	●			●						37

● - Si, ■ - Ge

The syntheses of the title phases use rare earth and silicon oxide reagents, necessitating the use of boron to remove oxygen from the reagents, thus leaving these elements available to

react with elemental selenium to form selenosilicates. Using NaI as flux we were able to obtain high-quality crystals of the $RE_3Mg_{0.5}SiSe_7$ series (RE = Ce, Pr, Nd, Sm, Gd, Tb, Dy), Figure 1. Although attempted several times, we were unable to prepare the La containing phase, even after changing the heating profile and the fluxes. We were also unable to obtain the compositions containing europium as well as rare earth elements smaller than dysprosium. Therefore, we surmise that the cerium to dysprosium containing composition represents the size limits for our target composition, and, as Eu prefers the +2 oxidation state in chalcogenides, we suspect that this is why the Eu containing phase failed to form. In all cases, the reaction products were washed with methanol. EDS analysis of $RE_3Mg_{0.5}SiSe_7$ (RE = Ce, Pr, Nd, Sm, Gd, Tb, Dy) confirmed the presence of all expected elements in the crystals Table S1.

To prepare phase pure polycrystalline samples, solid-state syntheses incorporating the BCM method were performed using the same starting reagent stoichiometries used in the flux synthesis and successfully synthesized powders of $RE_3Mg_{0.5}SiSe_7$ (RE = Ce, Pr, Nd, Sm, Gd) compounds. For the compound $RE_3Mg_{0.5}SiSe_7$ (RE = Ce, Nd), the powder exhibited complete phase purity. In the case of $RE_3Mg_{0.5}SiSe_7$ (RE = Pr, Sm, Gd) powders, along with the target composition, some minor RE_3Se_4 (RE = Pr, Sm) peaks and unidentified impurities for RE = Gd, Figure S1-S5 were found. In the case of $RE_3Mg_{0.5}SiSe_7$ (RE = Tb, Dy) several unidentified impurity peaks, Figure S6-S7 were found. Although many attempts were made using different reaction conditions, it was not possible to achieve the phase pure products of $RE_3Mg_{0.5}SiSe_7$ (RE = Pr, Sm, Gd, Tb, and Dy), since inevitably Pr_3Se_4, Sm_3Se_4, and some other unidentified impurities in the case of RE = Gd, Tb, Dy formed along with our target phases.

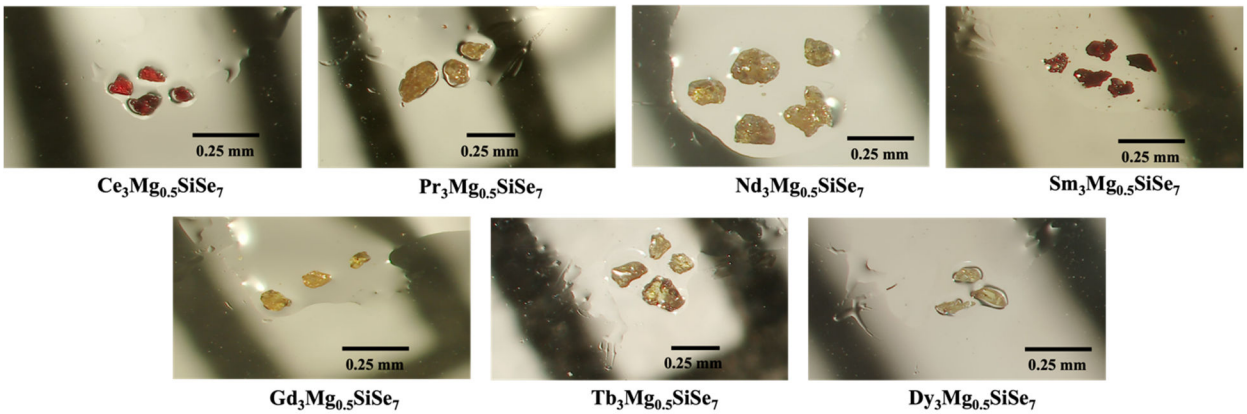

Figure 1. Optical images of $RE_3Mg_{0.5}SiSe_7$ (RE = Ce, Pr, Nd, Sm, Gd, Tb, Dy)

Crystal Structure.

The compounds of $RE_3Mg_{0.5}SiSe_7$ crystallize in the hexagonal crystal system in the space group $P6_3$ and are isostructural with the previously reported $RE_3M_{0.5}TQ_7$ family.[60] $RE_3Mg_{0.5}SiSe_7$ crystallizes in a 3D framework structure, where the rare earth cations are found in $RESe_8$ bicapped trigonal prisms that are edge- and face-shared with each other to create a ring-like structural motif. Within this motif the silicon edge shares to the bicapped trigonal prisms to form $SiSe_4$ tetrahedra. The magnesium is octahedrally coordinated in $MgSe_6$ octahedra that are face-shared to form infinite one-dimensional chains. These chains are located in the middle of the channels formed by the $RESe_8$ bicapped trigonal prisms and the isolated $SiSe_4$ tetrahedra are positioned to surround the assembly of $RESe_8$ bicapped trigonal prisms, Figure 2. The rare earth, silicon and selenium positions have 100% occupancy, while the magnesium site is 50% occupied in order to achieve charge balance. During the structure refinement, the Mg^{2+} occupancy factors were close to 0.5 for all the compounds and, consequently, to achieve charge balance, were fixed at 0.5.

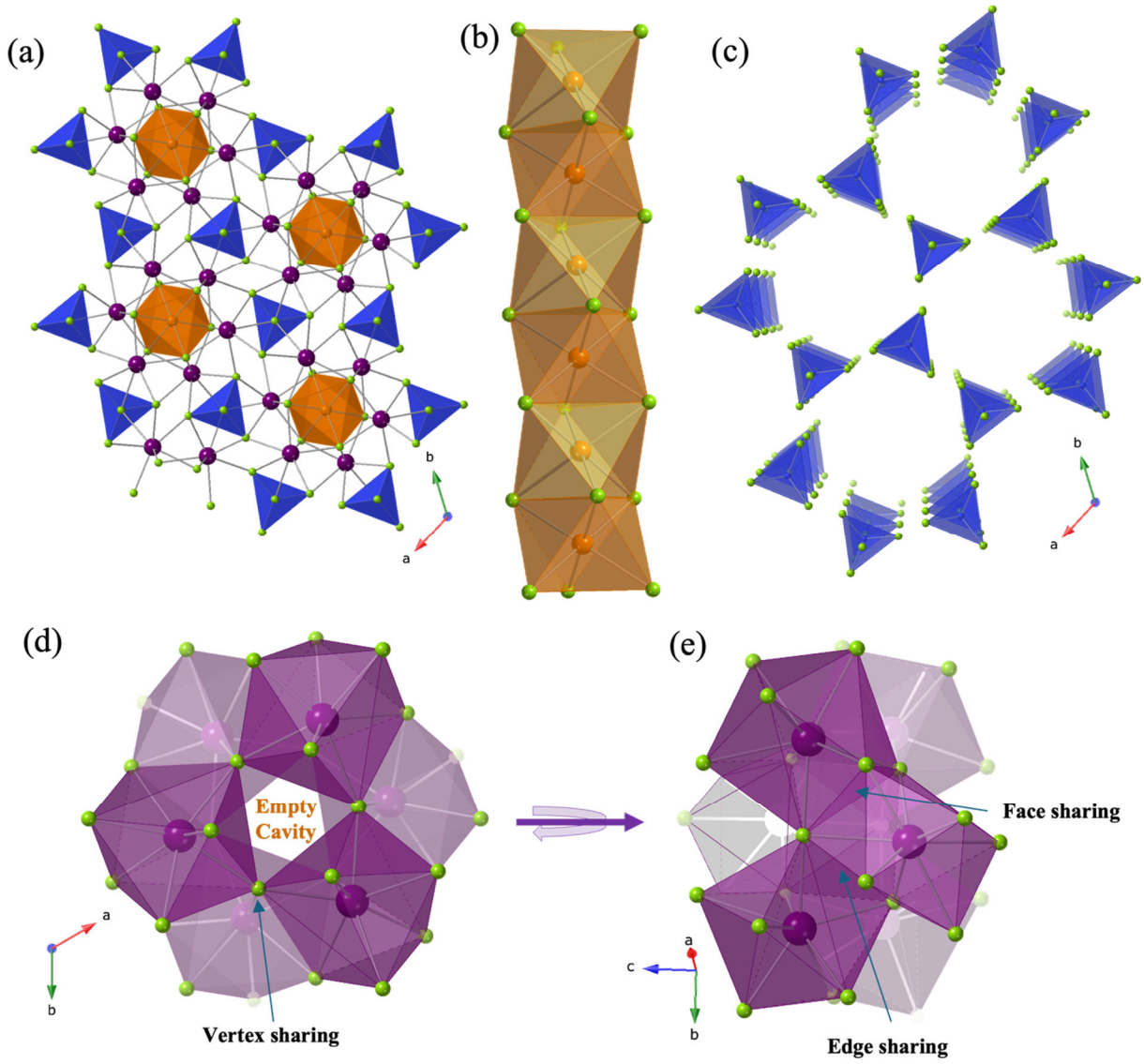

Figure 2. (a) 3D framework structure of $RE_3Mg_{0.5}SiSe_7$ viewed down the c-direction, (b) The one-dimensional chain of $MgSe_6$ octahedra extended along *c*-direction, (c) Isolated $SiSe_4$ tetrahedra in a ring-like formation, (d) and (e) The coordination environment of $RESe_8$ in $RE_3Mg_{0.5}SiSe_7$. Rare earth purple, silicon dark blue, magnesium orange, selenium light green.

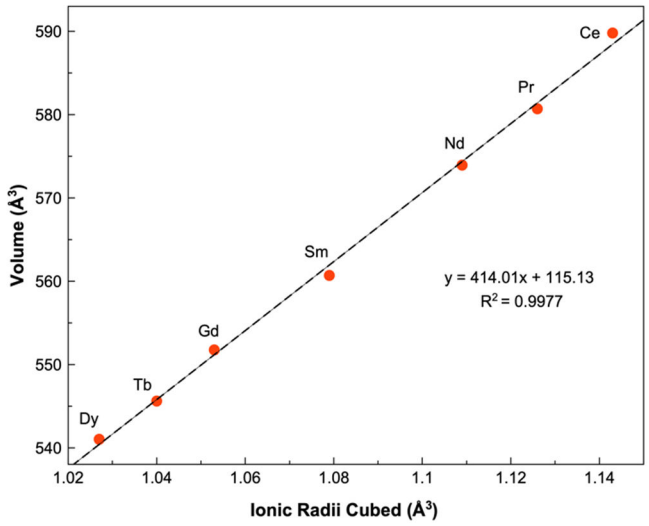

Figure 3. The dependence of the volume of $RE_3Mg_{0.5}SiSe_7$ compounds on the cubed ionic radii of the RE^{3+} elements.

The dependence of the unit cell volume of $RE_3Mg_{0.5}SiSe_7$ on the eight-coordinate Shannon ionic radii[61] of the rare earths is illustrated in Figure 3. The observed trend is consistent with the lanthanide contraction, where the gradual decrease of the unit cell volume is in good agreement with the decrease of the Shannon ionic radii of rare earth elements.

Magnetic Properties.

The magnetic susceptibility plots for $Ce_3Mg_{0.5}SiSe_7$ and $Gd_3Mg_{0.5}SiSe_7$ are shown in Figure 4. The inverse susceptibility data for $Ce_3Mg_{0.5}SiSe_7$ and $Gd_3Mg_{0.5}SiSe_7$ were fitted to the Curie−Weiss Law using the 100-300K temperature region to determine the magnetic moment and Weiss (θ_W) temperature. The observed and calculated magnetic moment and Weiss temperature results are summarized in Table 3.

Table 3. Summary of the Magnetic Data for $RE_3Mg_{0.5}SiSe_7$ (*RE* = Ce, and Gd)

Compound	Measured μ_{eff} (μ_B/RE^{3+})	Calculated μ_{eff} (μ_B/RE^{3+})	θ_W (K)
$Ce_3Mg_{0.5}SiSe_7$	2.97	2.54	-14.50 K
$Gd_3Mg_{0.5}SiSe_7$	7.29	7.98	-6.13 K

The effective magnetic moments calculated from the fits of the inverse magnetic susceptibility data agree with the calculated magnetic moments for Ce^{3+} and Gd^{3+} ions. The negative Weiss temperature observed for both compounds are consistent with antiferromagnetic correlations between neighboring rare-earth ions, however, no antiferromagnetic transitions are observed down to 2 K, Figure 4. For both $Ce_3Mg_{0.5}SiSe_7$ and $Gd_3Mg_{0.5}SiSe_7$ the field-cooled (fc) and zero field-cooled (zfc) data were the same; consequently just the zfc data are shown in Figure 4. These two compositions did not exhibit any indication of long-range magnetic order and, for that reason, magnetic measurements on the other compositions were not performed.

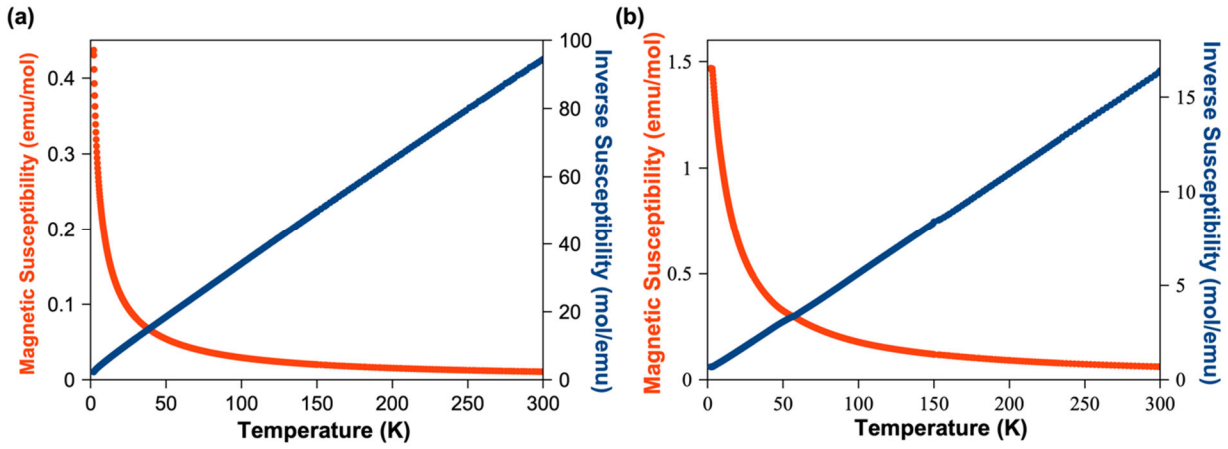

Figure 4. Molar susceptibility and inverse molar susceptibility vs temperature plots for polycrystalline $Ce_3Mg_{0.5}SiSe_7$ (a), and $Gd_3Mg_{0.5}SiSe_7$ (b).

UV−vis Diffuse Reflectance Spectroscopy.

The optical properties of the quaternary $RE_3Mg_{0.5}SiSe_7$ (*RE* = Ce, Pr, Nd, Sm, Gd) phases, were examined using polycrystalline powders and UV-vis plots are shown in Figure 5. The UV−vis absorption spectrum for $Nd_3Mg_{0.5}SiSe_7$ displays many weak absorption peaks due to the *f*–*f* electronic transitions of the Nd^{3+} cation. In the absorption spectrum of $Nd_3Mg_{0.5}SiSe_7$, Figure 5(a), the shoulder located at 886 nm corresponds to the multiplet $^4F_{3/2}$, and the broad band at 815 nm corresponds to the multiplet $^4F_{5/2}$. The absorption bands at 755 nm, 690 nm, a weak band at 630 nm, and the peak close to 590 nm correspond to the multiplets $^4F_{7/2}$, $^4F_{9/2}$, $^2H_{11/2}$, $^4G_{5/2}$, respectively. The observed transitions are consistent with literature data of the optical properties of Nd^{3+} ions by Jiang et al.[62] To convert the reflectance data for $RE_3Mg_{0.5}SiSe_7$ (RE = Ce, Pr, Sm, Gd) to absorption, the Kubelka−Munk equation was employed. Figure 5(b, c, d, and

e). The absorption plots are consistent with band gaps of 1.6(1) eV ($Ce_3Mg_{0.5}SiSe_7$), 1.7(1) eV ($Pr_3Mg_{0.5}SiSe_7$), 1.6(1) eV ($Sm_3Mg_{0.5}SiSe_7$), and 1.9(1) eV ($Gd_3Mg_{0.5}SiSe_7$), indicating the semiconducting nature of the studied selenosilicates. These bandgaps are consistent with the observed colors of the compounds.

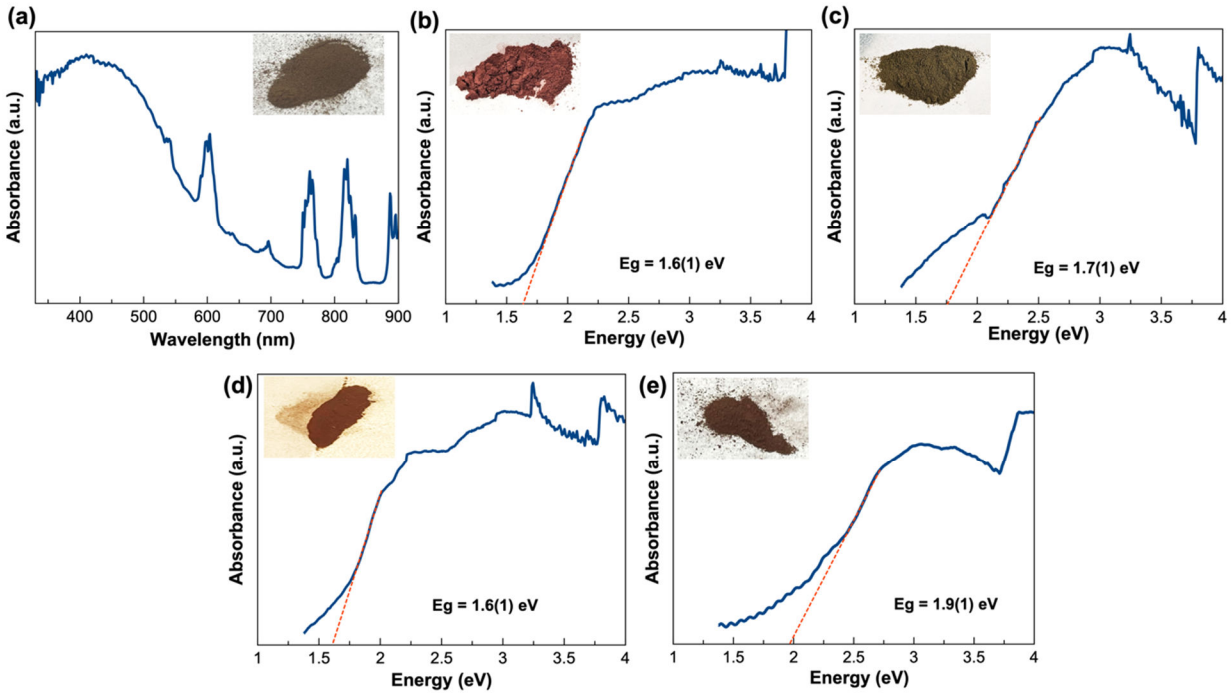

Figure 5. Optical absorption spectrum of polycrystalline $Nd_3Mg_{0.5}SiSe_7$ (a). The plots for $Ce_3Mg_{0.5}SiSe_7$ and $Pr_3Mg_{0.5}SiSe_7$, $Sm_3Mg_{0.5}SiSe_7$, $Gd_3Mg_{0.5}SiSe_7$, converted from the diffuse reflectance data to absorbance by the Kubelka-Munk function are shown in (b), (c), (d), and (e) respectively.

Second Harmonic Generation (SHG).

A multitude of reported $RE_3M_xTQ_7$ compositions crystallize in the noncentrosymmetric space group $P6_3$ and were investigated for their SHG properties.[63, 64] Yang *et al*. reported that La_3LiTS_7 (T = Ge, Sn) exhibits a strong NLO effect that is likely due to mixed contributions from the LnS_8 and TS_4 groups, where the quantified NLO contribution of LnS_8 is larger than that of the TS_4 group.[64] We decided to study the SHG properties of $Ce_3Mg_{0.5}SiSe_7$ and perform the flexibility index calculations to analyze quantitatively the mixed contribution of $CeSe_8$, and

$SiSe_4$ groups in SHG properties.[65] The flexibility index calculated for $CeSe_8$ (0.52) is greater than that of the $SiSe_4$ (0.28) group, suggesting that the contribution of the $CeSe_8$ group is larger than that of the $SiSe_4$ group in the SHG measurement, Table S2. The SHG properties of polycrystalline $Ce_3Mg_{0.5}SiSe_7$ powder were measured and SHG activity with an efficiency of ~0.11 times that of the KDP standard was observed. Figure 6 shows the time dependence of the SHG intensity for $Ce_3Mg_{0.5}SiSe_7$ and the KDP standard. The SHG response is weak, however, it confirms the noncentrosymmetric space group of $Ce_3Mg_{0.5}SiSe_7$.

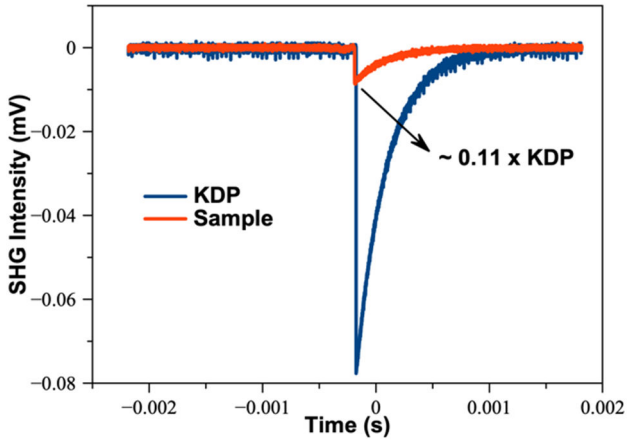

Figure 6. SHG intensity vs time of sample ($Ce_3Mg_{0.5}SiSe_7$) and KDP.

First-Principles Calculations:

The band gap values calculated by DFT are shown in Table S3. The DFT results confirm the semiconducting nature of these materials. However, the DFT values underestimate the bandgap observed by the experiment. Based on recent study in the use of r^2SCAN functional on a variety of materials, there is a tendency for slight underestimation of bandgap values of semiconductors.[54] This trend is consistent with the comparison between experimental and DFT bandgap in this study. To achieve a more accurate bandgap values, approaches such as the use hybrid functionals can be applied.[66, 67] However, we would like to note that these approaches would be much more costly and time consuming, thus the accurate calculation of electronic structure of these materials would be best reserved for a separate dedicated study. The total

density of states and band structures of $RE_3Mg_{0.5}SiSe_7$ (*RE* = Pr, Nd, Sm, Gd) are shown in Figures S8, and S9.

Conclusions

Seven quaternary rare earth magnesium selenosilicates, $RE_3Mg_{0.5}SiSe_7$ (*RE* = Ce, Pr, Nd, Sm, Gd, Tb, Dy), space group $P6_3$, were successfully prepared as single crystals, and represent new additions to the larger $RE_3M_{0.5}TQ_7$ family of compounds. High-quality single crystals were prepared by combining molten flux crystal growth with the BCM method and their structures determined by single crystal X-ray diffraction. Polycrystalline powders for property measurements were obtained by combining the BCM method with solid state synthesis. UV-vis measurements indicate the semiconducting nature of these materials, which was confirmed by DFT electronic structure calculations. Magnetic susceptibility measurements of $Ce_3Mg_{0.5}SiSe_7$ and $Gd_3Mg_{0.5}SiSe_7$ revealed paramagnetic behavior without any evidence of a magnetic transition down to 2K. Due to having a noncentrosymmetric space group, SHG behavior of $Ce_3Mg_{0.5}SiSe_7$ compound was measured, exhibiting SHG activity with an intensity 0.11 x KDP, confirming its assignment to a non-centrosymmetric space group. The versatility of this family that can readily accommodate numerous elements suggests potential future compositional expansion.

Notes

The authors declare no competing financial interest.

Associated Content

Supporting Information

The supporting information includes EDS tabulated data, PXRD patterns. This information is available free of charge at the website XXX.

The CCDC 2407215-2407221 entries encompass the supplementary crystallographic data associated with this paper. These data are accessible without charge through www.ccdc.cam.ac.uk/data_request/cif, or by sending a request via email to data_request@ccdc.cam.ac.uk, or by directly contacting The Cambridge Crystallographic Data Centre at 12 Union Road, Cambridge CB2 1EZ, UK; fax: +44 1223 336033. The supporting information (SI) file contains EDS results, and PXRD patterns of title compounds.

ACKNOWLEDGMENTS

The authors gratefully acknowledge the support from the U.S. Department of Energy, Office of Basic Energy Sciences, Division of Materials Sciences and Engineering, under award DE-SC0018739. Synthesis, structural characterization, optical and magnetic studies were conducted at the University of South Carolina. First-principles computations in this work were performed at the high-performance computing cluster, Hyperion, supported by the Division of Information Technology at the University of South Carolina. SHG measurements were performed at the University of Houston.

References.

(1) Berseneva, A. A.; zur Loye, H.-C. Advances in Chalcogenide Crystal Growth: Flux and Solution Syntheses, and Approaches for Postsynthetic Modifications. *Cryst. Growth & Des.* **2023**, *23*, 5368-5383.

(2) Messegee, Z. T.; Cho, J. S.; Craig, A. J.; Garlea, V. O.; Xin, Y.; Kang, C. J.; Proffen, T. E.; bhandari, H.; Kelly, J. C.; Ghimire, N. J.; Aitken, J. A.; Jang, J. I.; Tan, X. Multifunctional Cu_2TSiS_4 (T = Mn and Fe): Polar Semiconducting Antiferromagnets with Nonlinear Optical Properties. *Inorg. Chem.* **2022**, *62*, 530-542.

(3) Yuhas, B. D.; Smeigh, A. L.; Samuel, A. P. S.; Shim, Y.; Bag, S.; Douvalis, A. P.; Wasielewski, M. R.; Kanatzidis, M. G. Biomimetic Multifunctional Porous Chalcogels as Solar Fuel Catalysts. *J. Am. Chem. Soc.* **2011**, *133*, 7252-7255.

(4) Lekse, J. W.; Moreau, M. A.; McNerny, K. L.; Yeon, J.; Halasyamani, P. S.; Aitken, J. A. Second-Harmonic Generation and Crystal Structure of the Diamond-Like Semiconductors Li_2CdGeS_4 and Li_2CdSnS_4. *Inorg. Chem.* **2009**, *48*, 7516-7518.

(5) Zhou, W.; Yao, W. D.; Zhang, Q.; Xue, H.; Guo, S. P. Introduction of Li Into Ag-Based Noncentrosymmetric Sulfides for High-Performance Infrared Nonlinear Optical Materials. *Inorg. Chem.* **2021**, *60*, 5198-5205.

(6) Panigrahi, G.; Berseneva, A. A.; Morrison, G.; King, A. A.; Conner, R. L.; Jacobsohn, L. G.; zur Loye, H.-C. Crystal Growth of Quaternary $AkRE_2Si_2S_8$ (Ak = Ca and Sr; Re = La–Tb) Thiosilicates Using Flux-Assisted Boron Chalcogen Mixture Method: Exploring X-ray Scintillation, Luminescence, and Magnetic Properties. *Inorg. Chem.* **2024**, *63*, 12849-12857.

(7) Babo, J. M.; Choi, E. S.; Albrecht-Schmitt, T. E. Synthesis, Structure, Magnetism, and Optical Properties of $Cs_2Cu_3DyTe_4$. *Inorg. Chem.* **2012**, *51*, 11730-11735.

(8) King, A. A.; Breton, L. S.; Morrison, G.; Smith, M. D.; zur Loye, H.-C. Boron Chalcogen Mixture Method-Assisted Alkali Halide Flux Crystal Growth of an Extensive Family of Quaternary Rare Earth Transition-Metal Thiosilicates: Investigation of their Structures and Magnetic Properties. *Inorg. Chem.* **2023**, *62*, 18172-18178.

(9) Anand, A.; Zaffalon, M. L.; Cova, F.; Pinchetti, V.; Khan, A. H.; carulli, F.; Brescia, R.; Meinardi, F.; moreels, I.; Brovelli, S. Optical and Scintillation Properties of Record-Efficiency CdTe Nanoplatelets toward Radiation Detection Applications. *Nano Lett.* **2022**, *22*, 8900-8907.

(10) Kamaya, N.; Homma, K.; Yamakawa, Y.; Hirayama, M.; kanno, R.; Yonemura, M.; Kamiyama, T.; Kato, Y.; Hama, S.; Koji, K.; Mitsui, A. A Lithium Superionic Conductor. *Nat. Mater.* **2011**, *10*, 682-686.

(11) Kanno, R.; Murayama, M. Lithium Ionic Conductor Thio-LISICON: The Li2 S GeS_2 P_2S_5 System. *J. Electrochem. Soc.* **2001**, *148*, A742.

(12) Yu, Y.; Cagnoni, M.; Cojocaru-Mirédin, O.; Wuttig, M. Chalcogenide Thermoelectrics Empowered by an Unconventional Bonding Mechanism. *Adv. Funct. Mater.* **2020**, *30*, 1904862.

(13) Rogalski, A. HgCdTe Infrared Detector Material: History, Status and Outlook. *Rep. Prog. Phys.* **2005**, *68*, 2267-2336.

(14) Watanabe, S.; Ishikawa, S.; Aono, H.; Takeda, S.; Odaka, H.; Kokubun, M. High Energy Resolution Hard X-Ray and Gamma-Ray Imagers Using CdTe Diode Devices. *IEEE Trans. Nucl.* **2009**, *56*, 777 - 782.

(15) Lin, S. H.; Mao, J. G.; Guo, G. C.; Huang, J. S. Synthesis and Crystal Structure of a New Quaternary Compound: La_3AgSe_7Si. *J. Alloys Compd.* **1997**, *252*, L8-L11.

(16) Guo, S. P.; Guo, G. C.; Huang, J. S. Syntheses, Structures and Properties of Five Chiral Quaternary Sulfides, $Al_xLn_3(Si_yAl_{1-y})S_7$ (Ln = Y, Gd, Dy) and $In_{0.33}Sm_3SiS_7$. *Sci. China, Ser. B: Chem.* **2009**, *52*, 1609-1615.

(17) Breton, L. S.; Klepov, V. V.; zur Loye, H.-C. Facile Oxide to Chalcogenide Conversion for Actinides Using the Boron–Chalcogen Mixture Method. *J. Am. Chem. Soc.* **2020**, *142*, 14365-14373.

(18) Breton, L. S.; Baumbach, R.; Tisdale, H. B.; zur Loye, H.-C. Structures and Magnetic Properties of $K_2Pd_4U_6S_{17}$, $K_2Pt_4U_6S_{17}$, $Rb_2Pt_4U_6S_{17}$, $Cs_2Pt_4U_6S_{17}$ Synthesized Using the Boron–Chalcogen Mixture Method. *Inorg. Chem.* **2022**, *61*, 10502-10508.

(19) King, A. A.; Breton, L. S.; Morrison, G.; Smith, M. D.; zur Loye, H.-C. Boron Chalcogen Mixture Method-Assisted Alkali Halide Flux Crystal Growth of an Extensive Family of Quaternary Rare Earth Transition-Metal Thiosilicates: Investigation of Their Structural and Magnetic Properties. *Inorg. Chem.* **2023**, *62*, 18172-18178.

(20) Berseneva, A. A.; Klepov, V. V.; Kashem, H. B.; Maksimova, A. A.; Morrison, G.; Wright, J.; Schaeperkoetter, J.; Misture, S. T.; zur Loye, H.-C. Rare Bird: U^{+5} in Uranium Chalcogenides. *Chem. Mater.* **2024**, *36*, 7988-8001.

(21) Panigrahi, G.; Kashem, H. B.; Morrison, G.; zur Loye, H.-C. Synthesis of a Series of Rare-Earth-Based Multi-Anion Chalcogenide Iodides $Re_3Si_2Se_xS_{8-x}I$ (RE= La, Ce, Pr, and Nd) Using the Flux-Assisted Boron–Chalcogen Mixture Method. *Dalton Trans.* **2025**, *54*, 6252-6260.

(22) Michelet, A.; Flahaut, M. J. Sur Les Composes du Type $La_6MnSi_2S_{14}$. *C. R. Acad. Sci. Ser.* **1969**, *269*, 1203−1205.

(23) Collin, G.; Laruelle, P. Structure de $La_6Cu_2Si_2S_{14}$. *Bull. Soc. Fr. Mineral. cristallogr.* **1971**, *94*, 175−176.

(24) Jin, Z.; Li, Z.; Du, Y. Synthesis and the Crystal Structure of $La_6NiSi_2S_{14}$ and $La_6CoSi_2S_{14}$. *Chinese J. Appl. Chem.* **1985**, *2*, 42−46.

(25) Gulay, L. D.; Lychmanyuk, O. S.; Olekseyuk, I. D.; Pietraszko, A. Crystal Structures of the $R_3CuGeSe_7$ (R= Ce, Pr, Nd, Sm, Gd, Tb and Ho) Compounds. *J. Alloys Compd.* **2006**, *422*, 203-207.

(26) Huch, M. R.; Gulay, L. D.; Olekseyuk, I. D. Crystal Structures of the $R_3Mg_{0.5}GeS_7$ (R= Y, Ce, Pr, Nd, Sm, Gd, Tb, Dy, Ho and Er) Compounds. *J. Alloys Compd.* **2006**, *424*, 114-118.

(27) Gulay, L. D.; Lychmanyuk, O. S.; Olekseyuk, I. D.; Daszkiewicz, M.; Damm, S.; Pietraszko, A. Crystal Structures of the Compounds R_3CuSiS_7 (R= Ce, Pr, Nd, Sm, Tb, Dy and Er) and $R_3CuSiSe_7$ (R= La, Ce, Pr, Nd, Sm, Gd, Tb and Dy). *J. Alloys Compd.* **2007**, *431*, 185-190.

(28) Daszkiewicz, M.; Gulay, L. D.; Lychmanyuk, O. S.; Pietraszko, A. Crystal Structures of the $R_3Ag_{1-\delta}TSe_7$ (R= La–Nd, Sm, Gd–Dy, δ = 0–0.30; T = Ge, Si) Compounds. *J. Alloys Compd.* **2009**, *467*, 168-172.

(29) Yin, W.; Wang, W.; Kang, L.; Lin, Z.; Feng, K.; Shi, Y.; Hao, W.; Yao, J.; Wu, Y. Ln_3FeGaQ_7: A New Series of Transition-Metal Rare-Earth Chalcogenides. *J. Solid State Chem.* **2013**, *202*, 269−275.

(30) Daszkiewicz, M.; Pashynska, Y. O.; Marchuk…, O. V. Crystal Structure and Magnetic Properties of $R_3Co_{0.5}GeS_7$ (R= Y, La, Ce, Pr, Nd, Sm, Gd, Tb, Dy, Ho, Er and Tm) and $R_3Ni_{0.5}GeS_7$ (R= Y, Ce, Sm, Gd, Tb, Dy, Ho, Er, Tm). *J Alloys Compd.* **2015**, *647*, 445−455.

(31) Strok, O.; Daszkiewicz, M.; Gulay, L. Crystal Structure of $R_3Mg_{0.5}DSe_7$ (R = Ce, Pr; D = Si, Ge). *Chem. Met. Alloys.* **2015**, *8*, 16-21.

(32) Iyer, A. K.; Yin, W.; Lee, E. J.; Lin, X.; Mar, A. Quaternary Rare-Earth Sulfides $Re_3M_{0.5}GeS_7$ (Re= La–Nd, Sm; M= Co, Ni) and $Y_3Pd_{0.5}SiS_7$. *J. Solid State Chem.* **2017**, *250*, 14−23.

(33) King, A. A.; Breton, L. S.; Morrison, G.; Smith, M. D.; Liang, M.; Halasyamani, P. S.; zur Loye, H.-C. Crystal Structures and Property Measurements of Rare Earth Magnesium

Thiosilicates Synthesized via Flux Crystal Growth Utilizing the Boron Chalcogen Mixture (BCM) Method. *Inorg. Chem.* **2023**, *62*, 7446-7452.

(34) Gulay, L. D.; Lychmanyuk, O. S.; Olekseyuk, I. D.; Daszkiewicz, M.; damm, S.; Pietraszko, A. Crystal Structures of the Compounds R_3CuSiS_7 (R= Ce, Pr, Nd, Sm, Tb, Dy and Er) and $R_3CuSiSe_7$ (R= La, Ce, Pr, Nd, Sm, Gd, Tb and Dy). *J. Alloys Compd.* **2007**, *431*, 185-190.

(35) Wu, L. B.; Huang, F. Q. Crystal Structure of Trilanthanum Monosilver Monosilicon Heptasulfide, La_3AgSiS_7. *Z. Kristallogr. NCS*. **2005**, *220*, 307-308.

(36) Zhou, Y.; Iyer, A. K.; Oliynyk, A. O.; Heyberger, M.; Lin, Y.; Qiu, Y.; Mar, A. Quaternary Rare-Earth Sulfides $Re_3M_{0.5}M'S_7$ (M = Zn, Cd; M′ = Si, Ge). *J. Solid State Chem.* **2019**, *278*, 120914.

(37) He, J.; Wang, Z.; Zhang, X.; Cheng, Y.; Gong, Y.; Lai, X.; Zheng, C.; Lin, J.; Huang, F. Q. Synthesis, Structure, Magnetic and Photoelectric Properties of $Ln_3M_{0.5}M'Se_7$ (Ln = La, Ce, Sm; M = Fe, Mn; M′ = Si, Ge) and $La_3MnGaSe_7$. *RSC Adv.* **2015**, *5*, 52629-52635.

(38) Krause, L.; Herbst-Irmer, R.; Sheldric, G. M.; Stalke, D. Comparison of Silver and Molybdenum Microfocus X-Ray Sources for Single-Crystal Structure Determination. *J. Appl. Crystallogr.* **2015**, *48*, 3-10.

(39) Sheldrick, G. M. Shelxt–Integrated Space-Group and Crystal-Structure Determination. *Acta Crystallogr. A: Found. Adv.* **2015**, *71*, 3-8.

(40) Hübschle, C. B.; Sheldrick, G. M.; Dittrich, B. Shelxle: A Qt Graphical User Interface for SHELXL. *J. Appl. Cryst.* **2011**, *44*, 1281-1284.

(41) Dolomanov, O. V.; Bourhis, L. J.; Gildea, R. J.; Howard, J. A.; Puschmann, H. Olex2: A Complete Structure Solution, Refinement and Analysis Program. *J. Appl. Cryst. (***2009**, *42*, 339-341.

(42) Kubelka, P. Ein Beitrag zur Optik der Farbanstriche. *Z. technol. Phys.* **1931**, *12*, 593.

(43) Morrison, G.; zur Loye, H.-C. Simple Correction for the Sample Shape and Radial Offset Effects on Squid Magnetometers: Magnetic Measurements on Ln_2O_3 (Ln= Gd, Dy, Er) Standards. *J. Solid State Chem.* **2015**, *221*, 334-337.

(44) Kurtz, S. K.; Perry, T. T. A Powder Technique for the Evaluation of Nonlinear Optical Materials. *J. Appl. Phys.* **1968**, *39*, 3798-3813.

(45) Dougherty, J. P.; Kurtz, S. K. A Second Harmonic Analyzer for the Detection of Non-Centrosymmetry. *J. Appl. Cryst.* **1976**, *9*, 145-158.

(46) Blöchl, P. E. Projector Augmented-Wave Method. *Phys. Rev. B*. **1994**, *50*, 17953.

(47) Kresse, G.; Furthmüller, J. Efficient Iterative Schemes for Ab Initio Total-Energy Calculations Using a Plane-Wave Basis Set. *Phys. Rev. B.* **1996**, *54*, 11169-11186.

(48) Shishkin, M.; Marsman, M.; Kresse, G. Accurate Quasiparticle Spectra from Self-Consistent GW Calculations with Vertex Corrections. *Phys. Rev. Lett.* **2007**, *99*, 246403.

(49) Furness, J. W.; Kaplan, A. D.; Ning, J.; Perdew, J. P.; Sun, J. Accurate and Numerically Efficient r^{2}SCAN Meta-Generalized Gradient Approximation. *J. Phys. Chem. Lett.* **2020**, *11*, 8208-8215.

(50) Langreth, D. C.; Perdew, J. P. Theory of Nonuniform Electronic Systems. I. Analysis of the Gradient Approximation and a Generalization that Works. *Phys. Rev. B*. **1980**, *21*, 5469.

(51) Perdew, J. P.; Burke, K.; Ernzerhof, M. Generalized Gradient Approximation Made Simple. *Phys. Rev. Lett.* **1996**, *77*, 3865.

(52) Isaacs, E. B.; Wolverton, C. Performance of the Strongly Constrained and Appropriately Normed Density Functional for Solid-State Materials. *Phys. Rev. Materials*. **2018**, *2*, 063801.

(53) Kingsbury, R.; Gupta, A. S.; Bartel, C. J.; Munro, J. M.; Dwaraknath, S.; Horton, M.; Persson, K. A. Performance Comparison of r^2SCAN and SCAN metaGGA Density Functionals for Solid Materials via an Automated, High-Throughput Computational Workflow. *Phys. Rev. Materials*. **2022**, *6*, 013801.

(54) Kothakonda, M.; Kaplan, A. D.; Isaacs, E. B.; Bartel, C. J.; Furness, J. W.; Ning, J.; Wolverton, C.; Perdew, J. P.; Sun, J. Testing the r^{2}SCAN Density Functional for the Thermodynamic Stability of Solids with and without a Van Der Waals Correction. *ACS Mater. Au*. **2022**, *3*, 102-111.

(55) Monkhorst, H. J.; Pack, J. D. Special Points for Brillouin-Zone Integrations. *Phys. Rev. B*. **1976**, *13*, 5188-5192.

(56) Wisesa, P.; McGill, K. A.; Mueller, T. Efficient Generation of Generalized Monkhorst-Pack Grids through the Use of Informatics. *Phys. Rev. B*. **2016**, *93*, 155109.

(57) Pallikara, I.; Kayastha, P.; Skelton, J. M. The Physical Significance of Imaginary Phonon Modes in Crystals. *Electron. Struct.* **2022**, *4*, 033002.

(58) Togo, A. First-Principles Phonon Calculations with Phonopy and Phono3py. *J. Phys. Soc. Jpn.* **2023**, *92*, 012001.

(59) Togo, A.; Chaput, L.; Tadano, T.; Tanaka, I. Implementation Strategies in Phonopy and Phono3py. *J. Phys.: Condens. Matter*. **2023**, *35*, 353001.

(60) Zhou, Y.; Iyer, A. K.; Oliynyk, A. O.; Heyberger, M.; Lin, Y.; Qiu, Y.; Mar, A. Quaternary Rare-Earth Sulfides $Re_3M_{0.5}M'S_7$ (M = Zn, Cd; M′ = Si, Ge). *J. Solid State Chem.* **2019**, *278*, 120914.

(61) Shannon, R. D. T.; Prewitt, C. T. Effective Ionic Radii in Oxides and Fluorides. *Acta Crystallogr., Sect. B: Struct. Crystallogr. Cryst. Chem.* **1969**, *25*, 925- 946.

(62) Jiang, Z.; Yang, J.; Dai, S. Optical Spectroscopy and Gain Properties of Nd^{3+} - Doped Oxide Glasses. *JOSA B*. **2004**, *21*, 739-743.

(63) Shi, Y. F.; Chen, Y.; Chen, M. C.; Wu, L. M.; Lin, H.; Zhou, L. J.; Chen, L. Strongest Second Harmonic Generation in the Polar R_3MTQ_7 Family: Atomic Distribution Induced Nonlinear Optical Cooperation. *Chem. Mater.* **2015**, *27*, 1876-1884.

(64) Yang, Y.; Chu, Y.; Zhang, B.; Wu, K.; Pan, S. Unique Unilateral-Chelated Mode-Induced d–p−π Interaction Enhances Second-Harmonic Generation Response in New Ln_3LiMS_7 Family. *Chem. Mater.* **2021**, *33*, 4225-4230.

(65) Jiang, X.; Zhao, S.; Lin, Z.; Luo, J.; Bristowe, P. D.; Guan, X.; Chen, C. The Role of Dipole Moment in Determining the Nonlinear Optical Behavior of Materials: ab Initio Studies on Quaternary Molybdenum Tellurite Crystals. *J. Mater. Chem. C.* **2014**, *2*, 530.

(66) Perdew, J. P.; Zunger, A. Self-Interaction Correction to Density-Functional Approximations for Many-Electron Systems. *Phys. Rev. B*. **1981**, *23*, 5048.

(67) Shinde, R.; Yamijala, S. S.; Wong, B. M. Improved Band Gaps and Structural Properties from Wannier–Fermi–löwdin Self-Interaction Corrections for Periodic Systems. *J. Phys.: Condens. Matter*. **2020**, *33*, 115501.

For Table of Contents Use Only:

Crystal Growth of Quaternary Rare Earth Selenosilicates by Using the Flux-Assisted Boron Chalcogen Mixture Method: Investigation of their Magnetic and Optical Properties

Habiba Binte Kashem[1], Gopabandhu Panigrahi[1], Gregory Morrison[1], Eric A. Gabilondo[2], P. Shiv Halasyamani[2], and Hans-Conrad zur Loye[1*]

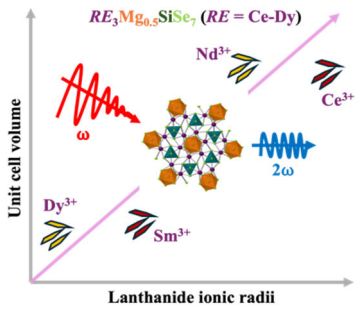

Synopsis:

Seven new rare earth magnesium-containing selenosilicates, $RE_3Mg_{0.5}SiSe_7$ (*RE* = Ce, Pr, Nd, Sm, Gd, Tb, Dy) were obtained via the flux assisted boron chalcogen mixture (BCM) method. Magnetic data revealed paramagnetic behavior in $Ce_3Mg_{0.5}SiSe_7$ and $Gd_3Mg_{0.5}SiSe_7$ with negative Weiss constant. The optical band gaps, determined from diffuse reflectance data, indicate the semiconducting nature of these materials which was confirmed by DFT electronic structure calculations. $Ce_3Mg_{0.5}SiSe_7$ was found to be SHG active with an efficiency of 0.11 times the standard potassium dihydrogen phosphate (KDP).